J|A|C|S
ARTICLES
Published on Web 09/14/2006

Giant Excitonic Zeeman Splittings in Colloidal Co^{2+}-Doped ZnSe Quantum Dots

Nick S. Norberg, Gregory L. Parks, G. Mackay Salley,† and Daniel R. Gamelin*

Contribution from the Department of Chemistry, Box 351700, University of Washington, Seattle, Washington 98195-1700

Received May 16, 2006; E-mail: Gamelin@chem.washington.edu

Abstract: Colloidal Co^{2+}:ZnSe diluted magnetic semiconductor quantum dots (DMS-QDs) were prepared by the hot injection method and studied spectroscopically. Ligand-field electronic absorption and magnetic circular dichroism (MCD) spectra confirm homogeneous substitutional speciation of Co^{2+} in the ZnSe QDs. Absorption spectra collected at various times throughout the syntheses reveal that dopants are absent from the central cores of the QDs but are incorporated at a constant concentration during nanocrystal growth. The undoped cores are associated with dopant exclusion from the ZnSe critical nuclei. Analysis of low-temperature electronic absorption and MCD spectra revealed excitonic Zeeman splitting energies (ΔE_{Zeeman}) of these Co^{2+}:ZnSe QDs that were substantially smaller than anticipated from bulk Co^{2+}:ZnSe data. This reduction in ΔE_{Zeeman} is explained quantitatively by the absence of dopants from the QD cores, where dopant−exciton overlap would be greatest. Since dopant exclusion from nucleation appears to be a general phenomenon for DMS-QDs grown by direct chemical methods, we propose that ΔE_{Zeeman} will always be smaller in colloidal DMS-QDs grown by such methods than in the corresponding bulk materials.

I. Introduction

Magnetic exchange interactions between paramagnetic dopant ions and semiconductor charge carriers (sp−d exchange) in diluted magnetic semiconductors (DMSs) give rise to numerous remarkable magnetic, optical, and magneto-transport properties such as giant Faraday rotations, giant Zeeman splittings of the semiconductor band structure, ferromagnetic ordering, and excitonic magnetic polarons.[1−3] These unusual magneto-electronic phenomena have generated a great deal of interest in this class of materials for potential spin-based information processing technologies ("spintronics"). There is particular interest in the influence of quantum confinement on sp−d exchange interactions since the changes in electronic structure induced by quantum confinement may offer a mechanism for manipulating the physical properties of DMSs. Recently, several groups have reported the use of direct chemical synthetic methods to prepare a variety of colloidal DMS nanocrystals,[4] including for example colloidal transition-metal (TM)-doped ZnO[5−7] and CdSe[8−10] (wurtzite), ZnS,[11,12] ZnSe,[10,13,14] and CdS[12,15,16] (cubic), PbSe[17] (rock salt), SnO_2[18] (rutile), and TiO_2[19] (anatase) nanocrystals. Whereas a great deal has been learned about the syntheses of such materials in recent years, relatively little research has addressed dopant−carrier exchange interactions in such colloidal DMS nanocrystals,[7,14,15] and in the few cases that have been studied, results relating to the influence of quantum confinement have been inconsistent. Strongly enhanced excitonic Zeeman splittings relative to bulk were reported for colloidal Mn^{2+}:ZnSe QDs prepared by hot injection,[14] but reduced splittings were reported for colloidal Mn^{2+}:CdS nanocrystals grown in inverted micelles.[15] Exchange energies reported for Co^{2+}:ZnO QDs[7] are between values reported for bulk Co^{2+}:ZnO,[20,21] but fewer measurements on the bulk form

† Permanent address: Department of Physics, Wofford College, Spartanberg, SC.

(1) Furdyna, J. K.; Kossut, J. Diluted Magnetic Semiconductors. In *Semiconductors and Semimetals*; Willardson, R. K., Beer, A. C., Eds.; Academic Press: New York, 1988; Vol. 25.
(2) Furdyna, J. K. *J. Appl. Phys.* **1988**, *64*, R29−R64.
(3) Kacman, P. *Semicond. Sci. Technol.* **2001**, *16*, R25−R39.
(4) Bryan, J. D.; Gamelin, D. R. *Prog. Inorg. Chem.* **2005**, *54*, 47−126.
(5) Norberg, N. S.; Kittilstved, K. R.; Amonette, J. E.; Kukkadapu, R. K.; Schwartz, D. A.; Gamelin, D. R. *J. Am. Chem. Soc.* **2004**, *126*, 9387−9398.
(6) Radovanovic, P. V.; Norberg, N. S.; McNally, K. E.; Gamelin, D. R. *J. Am. Chem. Soc.* **2002**, *124*, 15192−15193.
(7) Schwartz, D. A.; Norberg, N. S.; Nguyen, Q. P.; Parker, J. M.; Gamelin, D. R. *J. Am. Chem. Soc.* **2003**, *125*, 13205−13218.
(8) Hanif, K. M.; Meulenberg, R. W.; Strouse, G. F. *J. Am. Chem. Soc.* **2002**, *124*, 11495−11502. Magana, D.; Perera, S. C.; Harter, A. G.; Dalal, N. S.; Strouse, G. F. *J. Am. Chem. Soc.* **2006**, *128*, 2931−2939.
(9) Mikulec, F. V.; Kuno, M.; Bennati, M.; Hall, D. A.; Griffin, R. G.; Bawendi, M. G. *J. Am. Chem. Soc.* **2000**, *122*, 2532−2540.
(10) Erwin, S. C.; Zu, L. J.; Haftel, M. I.; Efros, A. L.; Kennedy, T. A.; Norris, D. J. *Nature* **2005**, *436*, 91−94.
(11) Bol, A. A.; Meijerink, A. *Phys. Rev. B.* **1998**, *58*, R15997−R16000.
(12) Radovanovic, P. V.; Gamelin, D. R. *J. Am. Chem. Soc.* **2001**, *123*, 12207−12214.
(13) Suyver, J. F.; Wuister, S. F.; Kelly, J. J.; Meijerink, A. *Phys. Chem. Chem. Phys.* **2000**, *2*, 5445−5448.
(14) Norris, D. J.; Yao, N.; Charnock, F. T.; Kennedy, T. A. *Nano Lett.* **2001**, *1*, 3−7.
(15) Hoffman, D. M.; Meyer, B. K.; Ekimov, A. I.; Merkulov, I. A.; Efros, A. L.; Rosen, M.; Couino, G.; Gacoin, T.; Boilot, J. P. *Solid State Commun.* **2000**, *114*, 547−550.
(16) Malik, M. A.; O'Brien, P.; Revaprasadu, N. *J. Mater. Chem.* **2001**, *11*, 2382−2386.
(17) Ji, T.; Jian, W.-B.; Fang, J. *J. Am. Chem. Soc.* **2003**, *125*, 8448−8449.
(18) Archer, P. I.; Radovanovic, P. V.; Heald, S. M.; Gamelin, D. R. *J. Am. Chem. Soc.* **2005**, *127*, 14479−14487.
(19) Bryan, J. D.; Heald, S. M.; Chambers, S. A.; Gamelin, D. R. *J. Am. Chem. Soc.* **2004**, *126*, 11640−11647.
(20) Pacuski, W.; Ferrand, D.; Cibert, J.; Deparis, C.; Gaj, J. A.; Kossacki, P.; Morhain, C. *Phys. Rev. B* **2006**, *73*, 035214.

of this material have been made. Theoretical studies predict a small reduction of effective exchange energies in the strong confinement regime[22] but an enhancement in the specific scenario of single dopant placement at the precise centers of the QDs.[15,23]

In this paper, we report the synthesis of colloidal Co^{2+}:ZnSe nanocrystals from monomeric precursors by hot injection and we investigate sp−d exchange interactions in these nanocrystals using magnetic circular dichroism (MCD) and electronic absorption spectroscopies. These spectroscopic techniques are used to evaluate the so-called "giant excitonic Zeeman splitting", which is the defining feature of a true DMS and is directly responsible for the appearance of strong MCD signals at the semiconductor band edge.[1,2,24] Co^{2+}:ZnSe has been studied extensively in its bulk form and its excitonic Zeeman splittings are well understood,[25,26] thus providing a firm calibration point for the present studies. Ligand-field electronic absorption and MCD spectroscopies were used to characterize Co^{2+} speciation and distribution within the ZnSe nanocrystals. These results reveal the presence of undoped ZnSe cores within the Co^{2+}:ZnSe QDs, an observation consistent with earlier results for colloidal Co^{2+}:ZnO[7,27] and Mn^{2+}:ZnSe[10] nanocrystals. The excitonic Zeeman splitting energies (ΔE_{Zeeman}) of these Co^{2+}:ZnSe QDs were found to be substantially smaller than anticipated from reported bulk Co^{2+}:ZnSe data. This discrepancy is explained quantitatively by the absence of Co^{2+} dopants from the central cores of the QDs, where exciton−dopant overlap would be greatest. A nonuniform dopant distribution within the DMS-QDs is thus concluded to be the dominant factor reducing the exitonic Zeeman splittings of these Co^{2+}:ZnSe nanocrystals relative to bulk. This scenario is anticipated to apply generally to all doped nanocrystals prepared by direct chemical synthesis from monomeric precursors.

II. Experimental Section

A. Materials. Zinc acetate dihydrate ($Zn(OAc)_2 \cdot 2H_2O$, 98%, <0.0005% magnetic impurities, Strem), cobalt acetate tetrahydrate ($Co(OAc)_2 \cdot 4H_2O$, 98.0%, GFS), oleic acid (OA, $C_{18}H_{36}O_2$, 97%, Acros), 1-hexadecylamine (HDA, $C_{16}H_{35}N$, 90%, Acros), 1-octadecene (ODE, $C_{18}H_{36}$, 90%, Aldrich), tributylphosphine (TBP, $C_{12}H_{27}P$, 97%, Aldrich), and selenium (Se, 99.5+%, Aldrich) were purchased and used as received.

B. Sample Preparation. The synthesis of Co^{2+}:ZnSe QDs was adapted from a procedure developed for pure ZnSe QDs.[28] A Zn/Co solution composed of 0.4 mmol of $(1 - x)Zn(OAc)_2 \cdot 2H_2O + xCo(OAc)_2 \cdot 4H_2O$, 1.2 mmol of OA, and 1.6 mmol of HDA in 16.0 g of ODE was purged with N_2 at 120 °C for about 1 h. A solution of 2.4 mmol of Se, 4 mmol of TBP, and 1.2 g of ODE was prepared in a glove box and stored under a N_2 atmosphere. The Zn/Co solution was heated to 310 °C, and the Se solution was rapidly injected using a gastight syringe. Following an initial drop in temperature after injection, the reaction solution was subsequently stabilized at 305 °C, where it was kept until the desired nanocrystal size was reached. Once the reaction solution cooled to <100 °C, the Co^{2+}:ZnSe nanocrystals were precipitated with a mixture of toluene and ethanol, centrifuged, and resuspended in toluene. Precipitation of the nanocrystals with ethanol and resuspension in toluene was repeated at least five times to remove excess reactants. Initially, the precipitate was oily, but subsequent washings resulted in progressively more powdery precipitates. These washed nanocrystals could be redispersed in nonpolar organic solvents.

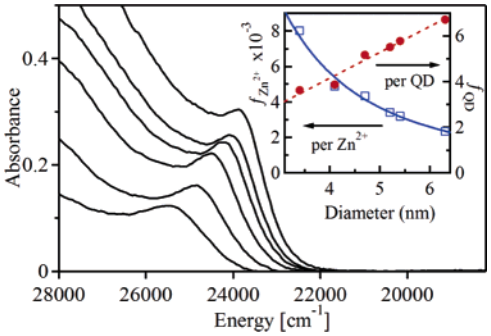

Figure 1. Electronic absorption spectra (300 K) of ZnSe nanocrystals removed from a reaction at different growth times (left to right: 1, 7, 15, 30, 46, and 70 min). Inset: The oscillator strengths of the ZnSe excitonic transitions measured per Zn^{2+} cation ($f_{Zn^{2+}}$, □) and per QD (f_{QD}, ●). The dotted line represents the best linear fit to f_{QD}. The solid curve is the same fit converted to a per Zn^{2+} basis.

C. Physical Measurements. Absorption spectra (300 K) of colloidal Co^{2+}:ZnSe QDs were collected using 1 cm cuvettes and a Cary 500 (Varian) spectrophotometer. Colloidal Co^{2+}:ZnSe nanocrystals were drop-coated onto quartz disks to form films for low-temperature electronic absorption and MCD measurements collected using an Aviv 40DS spectropolarimeter with a sample compartment modified to house a high-field superconducting magneto-optical cryostat (CryoIndustries SMC-1659M-OVT) positioned in the Faraday configuration. MCD intensities were measured as the absorbance difference ($\Delta A = A_L - A_R$, where L and R refer to left and right circularly polarized photons).

Powder X-ray diffraction data were collected using a Rigaku Rotaflex RTP300 X-ray diffractometer. TEM images were obtained using a JEOL 2010F transmission electron microscope. The Co^{2+} and Zn^{2+} concentrations in undoped and Co^{2+}:ZnSe QD dispersions were determined quantitatively using an inductively coupled plasma atomic emission spectrometer (ICP-AES, Jarrel Ash model 955) after acid digestion of the samples. Nanocrystal sizes were estimated from excitonic absorption peak energies using a previously reported relationship.[29]

III. Results

Figure 1 presents 300 K electronic absorption spectra of undoped ZnSe nanocrystals from aliquots collected during the course of a typical synthesis. Each aliquot was diluted by the same amount of toluene before recording the spectrum. The absorption peak, identified as the ZnSe excitonic transition, shifts to lower energy and increases in intensity with increasing reaction times. The excitonic energy at the end of the reaction is still significantly blue-shifted from bulk ZnSe (21 700 cm^{-1}, 2.69 eV).[30]

Figure 2 shows (a) high- and (b) low-resolution TEM images and (c) XRD data for Co^{2+}:ZnSe nanocrystals prepared as described above. The nanocrystals appear approximately spherical in shape with an average diameter of ca. 5 nm. Three broad

(21) Okabayashi, J.; Ono, K.; Mizuguchi, M.; Oshima, M.; Gupta, S. S.; Sarma, D. D.; Mizokawa, T.; Fujimori, A.; Yuri, M.; Chen, C. T.; Fukumura, T.; Kawasaki, M.; Koinuma, H. *J. Appl. Phys.* **2004**, *95*, 3573−3575.
(22) Bhattacharjee, A. K. *Phys. Rev. B.* **1998**, *58*, 15660−15665.
(23) Bhattacharjee, A. K.; Perez-Conde, J. *Phys. Rev. B* **2003**, *68*, 045303.
(24) Ando, K. *Science* **2006**, *312*, 1883−1885.
(25) Liu, X.; Petrou, A.; Jonker, B. T.; Krebs, J. J.; Prinz, G. A.; Warnock, J. *J. Appl. Phys.* **1990**, *67*, 4796−4797.
(26) Lascaray, J. P.; Hamdani, F.; Coquillat, D.; Bhattacharjee, A. K. *J. Magn. Magn. Mater.* **1992**, *104*, 995−996.
(27) Bryan, J. D.; Schwartz, D. A.; Gamelin, D. R. *J. Nanosci. Nanotech.* **2005**, *5*, 1472−1479.
(28) Li, L. S.; Pradhan, N.; Wang, Y.; Peng, X. *Nano Lett.* **2004**, *4*, 2261−2264.
(29) Smith, C. A.; Lee, H. W. H.; Leppert, V. J.; Risbud, S. H. *App. Phys. Lett.* **1999**, *75*, 1688−1690.
(30) Adachi, S.; Taguchi, T. *Phys. Rev. B.* **1991**, *43*, 9596−9577.

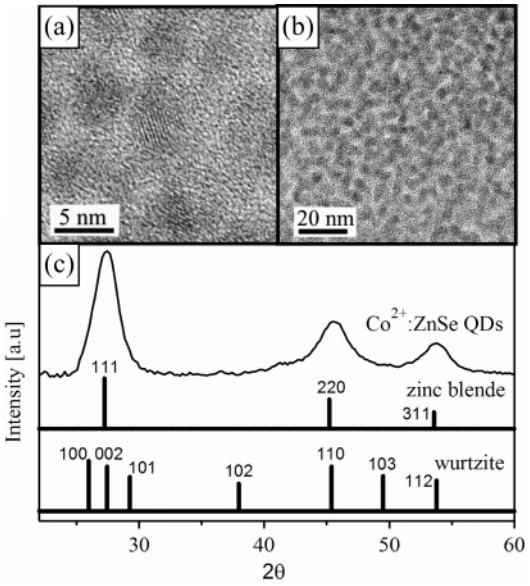

Figure 2. (a), (b) TEM images and (c) powder X-ray diffraction of Co^{2+}:ZnSe QDs. The powder diffraction patterns anticipated for zinc blende and wurtzite ZnSe are included in (c) for comparison.

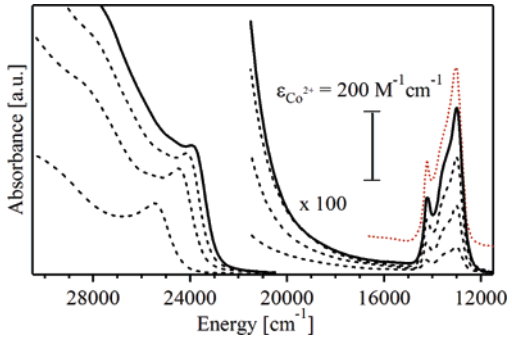

Figure 3. Electronic absorption spectra (300 K) of equivalent concentrations of washed Co^{2+}:ZnSe nanocrystals removed from the reaction mixture 0.5, 6, 15, and 30 min after injection of Se. The ligand field electronic absorption spectrum of bulk Co^{2+}:ZnSe ($^4A_2 \rightarrow {}^4T_1(P)$)[43] (···) is included for reference.

XRD peaks are observed that match those of zinc blende ZnSe but not wurtzite ZnSe. Scherrer analysis[31] of the XRD data yields average nanocrystal diameters consistent with those estimated by TEM and electronic absorption spectroscopy.

Figure 3 presents 300 K electronic absorption spectra of aliquots of washed colloidal Co^{2+}:ZnSe QDs extracted during the course of a typical synthesis (5% Co^{2+} precursor cation mole fraction). The absorption intensities are normalized to equal QD concentrations (as determined from analysis of Figure 1). The excitonic transition at 25 000 cm^{-1} shifts to lower energies with increasing reaction time. The absorption spectra of the washed samples before dilution show a structured feature centered at 13 500 cm^{-1} attributed to the $^4A_2(F) \rightarrow {}^4T_1(P)$ Co^{2+} ligand-field transition. This feature increases in intensity with increasing reaction time.

Figure 4a plots the relative number of Co^{2+} ions per QD versus the number of Zn^{2+} ions per QD for a series of aliquots taken during growth from two synthetic runs (solid markers). The number of Zn^{2+} ions per QD was estimated from the mean

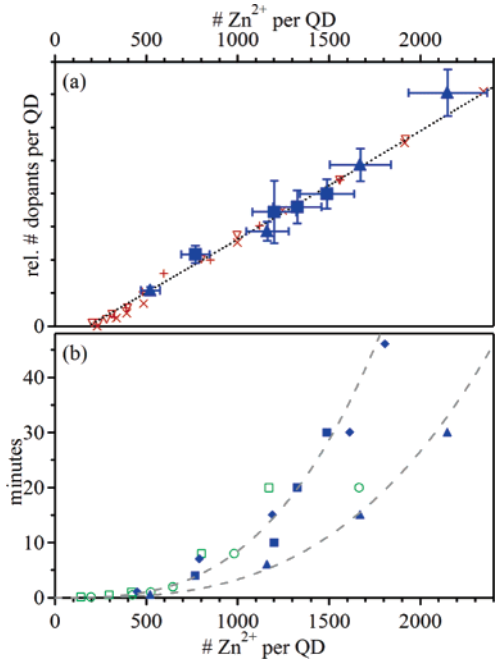

Figure 4. (a) Dopants per QD plotted vs Zn^{2+} cations per QD for two syntheses of Co^{2+}:ZnSe (▲ and ■) and adapted from data reported previously[10,32] for three syntheses of Mn^{2+}:ZnSe (+, ▽, and ×). Dotted line: A fit of the Co^{2+}:ZnSe data (see text). (b) Time after injection of Se vs Zn^{2+} cations per QD for the Co^{2+}:ZnSe QDs presented in (a), undoped ZnSe from Figure 1 (◆), and adapted from data reported previously[28] for synthesis of undoped ZnSe QDs (○ and □). Dashed lines: $dZn^{2+}/dt = Ct^{1/3}$.

nanocrystal diameters determined from their excitonic transition energies, and the number of Co^{2+} dopants was determined from the Co^{2+} ligand-field absorption intensities centered at 13 500 cm^{-1} after normalizing to equal QD concentrations (e.g., Figure 3). The error bars account for uncertainties in particle diameters, Co^{2+} absorption intensities, and the QD oscillator strengths. From Figure 4a, the number of Co^{2+} ions increases approximately linearly with the number of Zn^{2+} ions during growth. These data are essentially identical to analogous data reported previously[10,32] for the synthesis of Mn^{2+}:ZnSe by a similar method (also included in Figure 4a; +, ×, ▽). The solid markers in Figure 4b plot the reaction time versus the number of Zn^{2+} ions per QD for the pure ZnSe reaction (Figure 1) and both Co^{2+}:ZnSe reactions (Figure 4a). Zn^{2+} addition to the growing nanocrystals is most rapid immediately after injection, with QDs already containing ca. 500 Zn^{2+} ions only 30 s after injection. This growth rate slows considerably with increasing reaction times. This trend is the same as that observed previously for undoped ZnSe QDs prepared by a similar method (also included in Figure 4b; □ and ○).[28]

Figure 5 presents (a) 5 K electronic absorption and (b) 5 K, 1−6 T MCD spectra of 5.6 nm diameter, 0.77% Co^{2+}:ZnSe QDs. Three features are clearly evident in the MCD spectra: (i) a large, derivative-shaped MCD signal at 25 000 cm^{-1}, (ii) a negative feature just below the band gap at 23 000 cm^{-1}, and (iii) a highly structured sub-band gap feature centered at 13 700 cm^{-1}. The MCD signal intensities for all three features increase uniformly with magnetic field, as shown in the inset of Figure 5 (plotted on independently normalized *y* scales), indicating that

(31) West, A. R. *Solid State Chemistry and Its Applications*; John Wiley and Sons: New York, 1992.

(32) Zu, L.; Norris, D. J.; Kennedy, T. A.; Erwin, S. C.; Efros, A. L. *Nano Lett.* **2006**, *6*, 334−340.

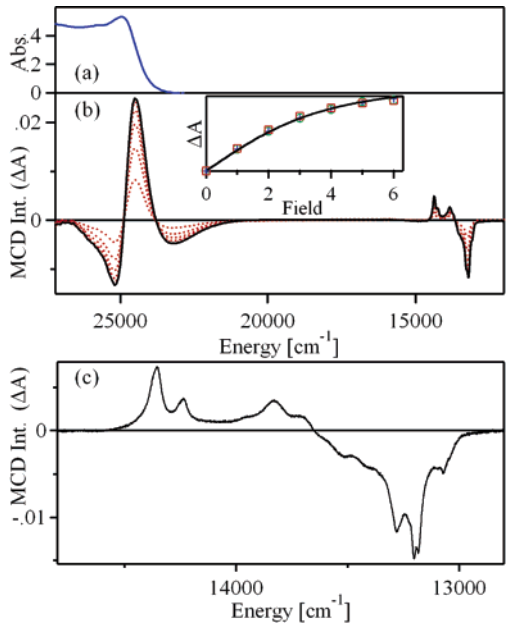

Figure 5. (a) 5 K electronic absorption and (b) 5 K, 1−6 T MCD spectra of 5.6 nm diameter 0.77% Co^{2+}:ZnSe QDs. (c) High-resolution MCD spectrum of the $^4A_2(F) \rightarrow {}^4T_1(P)$ Co^{2+} ligand-field transition collected at 5 K, 6 T. Inset: Normalized saturation magnetization of the Co^{2+} ligand field (□), excitonic (○), and charge-transfer (+) MCD intensities from part (b). The solid curve shows the spin-only saturation magnetization calculated from eq 1 using bulk Co^{2+}:ZnSe parameters[49] ($S = 3/2$ and $g = 2.27$).

all observed transitions originate from the same magnetic chromophore. Figure 5c shows a high-resolution MCD spectrum in the ligand field region, illustrating the rich structure of this feature.

IV. Analysis and Discussion

A. Excitonic Oscillator Strengths of ZnSe QDs. To assist analysis of the synthesis and magneto-optical spectra of the Co^{2+}:ZnSe QDs, the excitonic oscillator strengths of undoped ZnSe QDs were determined. Relative excitonic oscillator strengths were first measured by monitoring the excitonic absorption during growth of a single reaction of ZnSe nanocrystals prepared by hot injection (Figure 1). In this procedure, rapid nucleation is followed by growth under conditions where no more nanocrystals are nucleated,[33,34] and the total number of nanocrystals in the reaction mixture is thus constant. The absence of continued nucleation is confirmed by the fact that the width of the ZnSe QD excitonic absorption band decreases during growth. This indicates that the size distribution of the QDs is also decreasing (focusing),[35] which is only possible if no new nanocrystals are nucleated after the initial injection. The rising excitonic absorption intensity with nanocrystal growth in Figure 1 therefore provides direct evidence that the excitonic oscillator strengths of ZnSe nanocrystals increase with increasing size in this size range (∼3−6 nm diameters).

Integration of the Gaussian-resolved excitonic bands with respect to measured Zn^{2+} concentrations for the various particle sizes yielded excitonic oscillator strengths per QD (f_{QD}) and per Zn^{2+} ($f_{Zn^{2+}}$) as a function of nanocrystal diameter (Figure 1 inset). A straight-line (dashed) fit the f_{QD} data (circles) well over this size range ($f_{QD} = 1.14$(diameter in nm) $- 0.397$), and this fit was converted to yield the curved line (solid) passing through the $f_{Zn^{2+}}$ data (squares). Importantly, $f_{Zn^{2+}}$ for the QDs approaches its bulk value (1×10^{-3} at 190 K)[36] asymptotically as the nanocrystal diameter increases, confirming the data analysis.

The general trends in both f_{QD} and $f_{Zn^{2+}}$ are similar to data reported for other II-VI QD systems.[37,38] The complete overlap between the excitonic electron and hole wavefunctions in the limit of strong quantum confinement implies that $f_{Zn^{2+}}$ should be proportional to $(2a_B/d_{nc})^3$ if the QDs were in this regime (a_B is the excitonic Bohr radius, d_{nc} is the nanocrystal diameter), i.e., f_{QD} should be independent of d_{nc} in the strong quantum confinement regime.[39] Such behavior was observed in CdS nanocrystals when d_{nc} was much smaller than the CdS excitonic Bohr radius ($d_{nc} < a_B$), but a weaker dependence of $f_{Zn^{2+}}$ on d_{nc} was observed at larger sizes.[37] With $a_B = 2.3$ nm calculated[40] for ZnSe from its electron and hole effective masses[41] and dielectric constant,[30] the nanocrystals presented in Figure 1 (3.0 nm $< d_{nc} <$ 6.5 nm) are clearly in the weak confinement regime and thus not small enough to follow the relationship $f_{Zn^{2+}} \propto (2a_B/d_{nc})^3$. Instead, $f_{Zn^{2+}}$ decreases more gradually (and f_{QD} increases) with increasing d_{nc} in these weakly confined ZnSe QDs.

B. Synthesis of Co^{2+}:ZnSe QDs. The ZnSe nanocrystals prepared in the presence of Co^{2+} were similar to those prepared without Co^{2+}, with approximately spherical shapes and average diameters ranging from 3 to 6 nm as confirmed by TEM, XRD, and electronic absorption spectroscopy (Figure 2). Although both zinc blende and wurtzite ZnSe nanocrystals have reportedly been synthesized by hot injection,[28,42] the XRD data confirm that the DMS-QDs synthesized here are zinc blende (Figure 2c).

Incorporation of Co^{2+} into the ZnSe QDs during growth is evident from the increasing $^4A_2(F) \rightarrow {}^4T_1(P)$ ligand-field absorption intensity per QD with increasing nanocrystal size (Figure 3). The Co^{2+} $^4T_1(P)$ absorption bands of the washed samples all match that of bulk cubic Co^{2+}:ZnSe[43] closely (Figure 3, dotted), confirming that Co^{2+} is substitutionally doped into the cubic ZnSe nanocrystal lattices. No other Co^{2+} species could be detected. The sensitivity of ligand-field electronic absorption spectroscopy to changes in Co^{2+} speciation has previously allowed differentiation between surface-bound and internally doped Co^{2+} in Co^{2+}:ZnO[6,7] and Co^{2+}:CdS[12] QDs. Ligand-field absorption and electron paramagnetic resonance spectra were also used to demonstrate removal of surface-bound dopants by coordinating solvents such as TOPO, DDA, or pyridine.[5,7,9,12] Although no extra surface-cleaning step was performed in the present synthesis, it is evident from the data in Figure 3 that the HDA and oleic acid used in this synthesis are capable of

(33) Dushkin, C. D.; Saita, S.; Yoshie, K.; Yamaguchi, Y. *Adv. Colloid Interface Sci.* **2000**, *88*, 37−78.
(34) Murray, C. B.; Norris, D. J.; Bawendi, M. G. *J. Am. Chem. Soc.* **1993**, *115*, 8706−8715.
(35) Peng, X. G.; Wickham, J.; Alivisatos, A. P. *J. Am. Chem. Soc.* **1998**, *120*, 5343−5344.
(36) Zheng, J.-Z.; Allen, J. W. *Adv. Mater. Opt. Electr.* **1994**, *3*, 137−140.
(37) Vossmeyer, T.; Katsikas, L.; Giersig, M.; Popovic, I. G.; Diesner, K.; Chemseddine, A.; Eychmuller, A.; Weller, H. *J. Phys. Chem.* **1994**, *98*, 7665−7673.
(38) Yu, W. W.; Qu, L.; Guo, W.; Peng, X. *Chem. Mater.* **2003**, *15*, 2854−2860.
(39) Wang, Y.; Herron, N. *J. Phys. Chem.* **1991**, *95*, 525−532.
(40) Weisbuch, C.; Vinter, B. *Quantum Semiconductor Structures*; Academic Press: San Diego, 1991.
(41) Riccius, H. D.; Turner, R. *J. Phys. Chem. Solids* **1967**, *28*, 1623−1624. Marple, D. T. F. *J. Appl. Phys.* **1964**, *35*, 1879−1882.
(42) Reiss, P.; Quemard, G.; Carayon, S.; Bleuse, J.; Chandezon, F.; Pron, A. *Mater. Chem. Phys.* **2004**, *84*, 10−13.
(43) Tsai, T. Y.; Birnbaum, M. *J. Appl. Phys.* **2000**, *87*, 25−29.

stripping Co^{2+} ions from the ZnSe nanocrystal surfaces, thereby yielding internally doped Co^{2+}:ZnSe QDs with no surface-exposed Co^{2+} ions.

The combination of Co^{2+} ligand-field absorption intensities and ZnSe QD oscillator strengths allows a direct quantitative determination of Co^{2+} incorporation into the QDs during growth. This is best demonstrated by plotting the relative number of substitutional Co^{2+} ions per QD versus the number of Zn^{2+} ions per QD as in Figure 4a (solid markers). In the limit of purely statistical incorporation, this plot should be linear and intersect the origin. The fact that the data in Figure 4a are linear reveals that Co^{2+} is incorporated at a constant concentration during ZnSe growth. The Co^{2+} does not react at the same absolute rate as Zn^{2+}, however, since the Co^{2+}/Zn^{2+} ratios in the QDs are only 10−20% of the starting solution ratios according to ICP-AES analysis. This small Co^{2+}/Zn^{2+} incorporation ratio (effective segregation coefficient) cannot derive from an ionic radius mismatch since Co^{2+} and Zn^{2+} have essentially identical tetrahedral ionic radii. Instead, it is attributed to the competition between surface Se^{2-} and solvated ligands (HDA, oleic acid) for Co^{2+} ligation relative to that for Zn^{2+} ligation. The slow concentration of Co^{2+} in the nutrient relative to Zn^{2+} because of segregation raises the possibility that Co^{2+} may be incorporated at a higher concentration during the later stages of QD growth as its solution concentration builds up. Evidence of a dopant concentration gradient is not observed in Figure 4a, though. Quantitative analysis indicates that less than 10% of the original cation ($Zn^{2+} + Co^{2+}$) nutrient had been consumed even for the largest nanocrystals. The best fit of the data in Figure 4a accounting for Co^{2+} enrichment of the nutrient (dotted line) thus effectively yields a straight line, indicative of a constant Co^{2+} concentration throughout the nanocrystal growth volume.

Interestingly, the data in Figure 4a do not intersect the origin, as would be expected if Co^{2+} ions were incorporated at the same concentration throughout the entire volumes of the nanocrystals. From extrapolation of the fit to zero Co^{2+}, these data suggest the central 181 ± 109 cation sites of the QDs contain no Co^{2+} dopants, corresponding to an estimated undoped core diameter of 2.5 nm (1.8 nm < diameter < 2.9 nm). Two other recent reports have also revealed evidence of dopant exclusion from the centers of DMS-QDs grown by direct chemical methods: In wurtzite Co^{2+}:ZnO nanocrystals grown from solution, Co^{2+} ions were found to be quantitatively excluded from the critical nuclei, but were readily incorporated during nanocrystal growth.[7] From quantitative analysis of nucleation inhibition data, the critical nuclei were estimated to be 25 ± 4 Zn^{2+} cations, or ca. 1 nm in diameter.[27] Subsequently, an undoped core of about 2.5 nm diameter was observed for Mn^{2+}:ZnSe QDs prepared by hot injection, as determined by photoluminescence, EPR spectroscopy, and ICP-AES.[10,32] Data plotting the number of Mn^{2+} ions per QD versus the number of Zn^{2+} ions per QD adapted from refs 10 and 32 are included in Figure 4a (+, ×, ▽) for comparison and agree remarkably well with the present results for Co^{2+}:ZnSe. The linearity of these Mn^{2+}:ZnSe data also indicates dopant incorporation at a constant concentration during nanocrystal growth, as described for Co^{2+}:ZnSe above. Furthermore, the agreement between these two data sets substantiates the implicit assumption of a $^4T_1(P)$ ligand-field oscillator strength that is independent of particle size over the range presented in Figure 4a.

Dopant incorporation into the growing nanocrystals is not highly dependent on the absolute growth rates of the QDs. Figure 4b plots kinetics data for several Co^{2+}:ZnSe and ZnSe QD reactions, including some previously published ZnSe QD data from the same synthesis method.[28] For comparison purposes, these data are plotted using the same x axis as in Figure 4a. In all cases, growth is rapid immediately following injection but slows considerably as the nanocrystals increase in size. Each individual data set follows approximately the phenomenological rate law of $dZn^{2+}/dt = Ct^{1/3}$ (dashed lines). Small variations in experimental parameters (e.g., temperatures, concentrations, etc.) likely cause the variations in the absolute growth rate from experiment to experiment. The important conclusion drawn from comparison of these data with those of Figure 4a is that the effective Co^{2+}/Zn^{2+} incorporation ratio (effective segregation coefficient) is constant over an order of magnitude range of absolute growth rates, demonstrating that nanocrystal growth kinetics are not the origin of the undoped cores.

On the basis of our prior experience with Co^{2+}:ZnO,[7,27] we propose that the existence of undoped ZnSe cores in these Co^{2+}:ZnSe QDs arises from exclusion of dopants from the critical nuclei of the ZnSe nanocrystals. Detailed analysis of the Co^{2+}:ZnO QD synthesis showed that the nucleation is highly sensitive to impurities.[27] For example, the incorporation of a single Co^{2+} dopant during ZnO nucleation was estimated to slow the rate of nucleation by 1.5×10^4, effectively resulting in nucleation of only the pure ZnO nanocrystals. We suggested that this scenario will likely occur for all DMS-QDs grown by direct synthetic methods from monomeric precursors.[27] We thus associate the undoped ZnSe core with the ZnSe critical nucleus. Band gap energies reported in related syntheses suggest that stable ZnSe nanocrystals of ≤2 nm in diameter can be prepared.[44] We therefore place an upper limit of ca. 2 nm on the size of the critical nucleus for ZnSe grown by this method, which is within error of the undoped core diameter estimated from the data in Figure 4a (1.8 nm < d_{core} < 2.9 nm). Although this diameter is large compared to the 1 nm critical nucleus diameter found for ZnO,[27] it is comparable to those estimated for CdSe QDs (from 1.6 to 2.0 nm) from growth studies under conditions similar to those used here.[33,45] These conclusions are summarized schematically in Figure 6, which replots the data from Figure 4a as the probability of dopant incorporation versus the number of Zn^{2+} ions per QD (circles). Dopants have zero probability of being incorporated in the critical nucleus but have a constant nonzero probability of incorporation during growth (i.e., constant Co^{2+} concentration), resulting in QDs with pure ZnSe cores and homogeneous Co^{2+}-doped ZnSe shells (Figure 6).

C. Electronic Structure of Co^{2+}:ZnSe QDs. MCD spectroscopy provides a direct approach to evaluating the essential properties of DMSs by probing the interaction between magnetic ions and their semiconductor host[2] while eliminating potential complications arising from very small amounts of impurities that can dominate magnetic susceptibilities and go undetected

(44) Cumberland, S. L.; Hanif, K. M.; Javier, A.; Khitrov, G. A.; Strouse, G. F.; Woessner, S. M.; Yun, C. S. *Chem. Mater.* **2002**, *14*, 1576−1584. Hines, M. A.; Guyot-Sionnest, P. *J. Phys. Chem. B.* **1998**, *102*, 3655−3657.
(45) Bullen, C. R.; Mulvaney, P. *Nano Lett.* **2004**, *4*, 2303−2307.

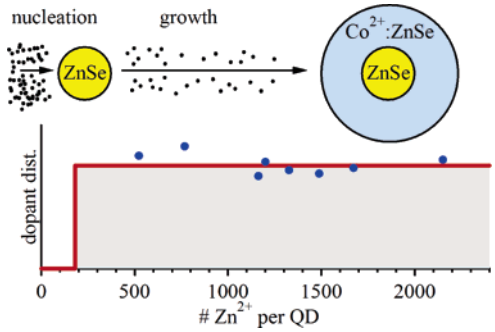

Figure 6. Summary of experimental dopant distribution within the Co^{2+}:ZnSe QDs determined from Figure 4. The synthesis is characterized by dopant exclusion from nucleation (first 181 Zn^{2+} ions) followed by statistical dopant inclusion during growth. The data from Figure 4a (●) are included for illustration.

by structural techniques such as X-ray diffraction.[24] MCD spectroscopy was therefore used to probe the electronic structures of the Co^{2+}:ZnSe DMS-QDs prepared here. Three main features are observed in the MCD spectra of the Co^{2+}:ZnSe QDs (Figure 5). The lowest energy feature centered at ca. 13 700 cm^{-1} is readily attributable to the Co^{2+} $^4A_2 \rightarrow {}^4T_1(P)$ ligand field transition. This band shows extensive fine structure in the high-resolution 5 K MCD spectrum presented in Figure 5c. The complex structure of this band arises primarily from the first-order spin−orbit splitting of the $^4T_1(P)$ excited state, with additional intensity contributions arising from the nearby $^2T_1$ and ^2E states.[46] The small line widths of only ∼15 cm^{-1} near the first electronic origin reflect the Co^{2+} structural homogeneity.

The large derivative MCD feature at ca. 25 000 cm^{-1} (Figure 5) is associated with the first excitonic transition of ZnSe. Its large MCD intensity is a manifestation of strong sp−d exchange coupling, as discussed in Section IV.D.

The broad, negative MCD feature just below the band gap (∼23 000 cm^{-1}) is attributed to a charge-transfer transition involving the Co^{2+} dopants. This MCD feature is not observed in undoped ZnSe (data not shown) or Mn^{2+}:ZnSe[14] QDs, confirming its identification as a transition distinct from the excitonic transition and associated with Co^{2+}. Detailed analysis of this feature to be reported elsewhere[47] demonstrates its assignment as a metal-to-conduction-band charge transfer (or donor-type photoionization) transition, consistent with previous assignments in bulk Co^{2+}:ZnSe based on photocapacitance and transient absorption measurements.[48]

The normalized 5 K MCD intensities of all three energy regions are plotted as a function of field in the inset of Figure 5. All three features show the same saturation magnetization curve. This curve is reproduced well by the $S = 3/2$ Brillouin function (eq 1) using the isotropic g-value for bulk Co^{2+}:ZnSe ($g = 2.27$),[49] where M is magnetization, N is the number of

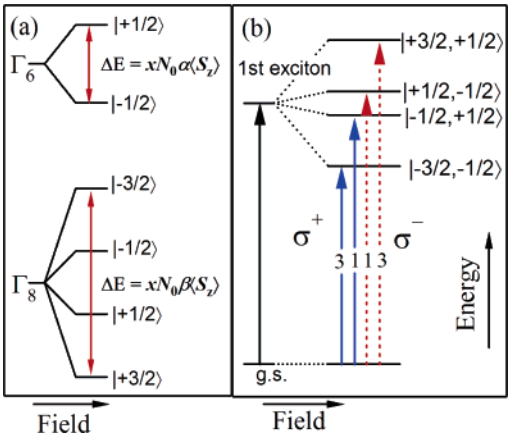

Figure 7. (a) Zeeman splittings of the semiconductor valence (Γ_8) and conduction (Γ_6) bands in cubic ZnSe. The splitting energies depend on dopant concentration (x), the dopant−carrier exchange coupling energies ($N_0\beta$ and $N_0\alpha$), and the average spin expectation value of the magnetic ion along the external field in the z direction ($\langle S_z \rangle$). (b) The absorption transitions allowed by MCD spectroscopy in the Faraday configuration, depicted along with their relative intensities for right (σ^+) and left (σ^-) circularly polarized photons.

paramagnetic ions, μ_B is the bohr magneton, H is magnetic field, k is Boltzmann's constant, and T is temperature.

$$M = \frac{1}{2} Ng\mu_B \left[(2S + 1) \coth\left((2S + 1)\left(\frac{g\mu_B H}{2kT}\right)\right) - \coth\left(\frac{g\mu_B H}{2kT}\right)\right] \quad (1)$$

The identical saturation of all three transitions confirms that these MCD intensities are all attributable to substitutionally doped Co^{2+} in the ZnSe lattice.

D. Excitonic Zeeman Splittings. i. Background. ZnSe is a direct-gap zinc blende semiconductor with a Γ_6 ($J = 1/2$) conduction band minimum and a Γ_8 ($J = 3/2$) valence band maximum (Figure 7a).[2] Following Furdyna,[1,2] the excitonic transition can be described using a one-electron picture in which the valence band splits into four Zeeman components and the conduction band splits into two Zeeman components in an applied magnetic field (Figure 7a). In the presence of magnetic dopants, the splittings of the conduction and valence bands of the semiconductor will be greatly enhanced due to sp−d exchange interactions, parametrized by $N_0\alpha$ (potential exchange coupling between the conduction band carrier and the dopant, s−d exchange) and $N_0\beta$ (kinetic exchange coupling between the valence band carrier and the dopant, p−d exchange). Following the selection rule of $\Delta m_J = \pm 1$ for MCD in the Faraday geometry (Figure 7b), four transitions with relative intensities of 3:1:−1:−3 are anticipated.[1,50] Nonzero $N_0\alpha$ and $N_0\beta$ values lead to excitonic Zeeman splittings ($|+3/2,+1/2\rangle - |-3/2,-1/2\rangle$) as described by eq 2,

$$\Delta E_{\text{Zeeman}} = x\langle S_z \rangle N_0(\alpha - \beta) \quad (2)$$

where x is the fractional dopant concentration, corrected for statistical dimer formation,[4] and $\langle S_z \rangle$ is the spin expectation value of the magnetic ions in the direction of the applied magnetic field. The intrinsic excitonic Zeeman splittings of pure ZnSe are much smaller than those induced by sp−d exchange and are therefore neglected in eq 2.

(46) Baranowski, J. M.; Allen, J. W.; Pearson, G. L. *Phys. Rev.* **1967**, *160*, 627−632.
(47) Norberg, N. S.; Dalpian, G. M.; Chelikowsky, J. R.; Gamelin, D. R. Submitted for publication.
(48) Noras, J. M.; Szawelska, H. R.; Allen, J. W. *J. Phys. C: Solid State Phys.* 1981, *14*, 3255−3268. Ehlert, A.; Dreyhsig, J.; Gumlich, H.-E.; Allen, J. W. *J. Lumin.* **1994**, *60−61*, 21−25.
(49) Ham, F. S.; Ludwig, G. W.; Watkins, G. D.; Woodbury, H. H. *Phys. Rev. Lett.* **1960**, *5*, 468−470.
(50) Alawadhi, H.; Miotkowski, I.; Souw, V.; McElfresh, M.; Ramdas, A. K.; Miotkowska, S. *Phys. Rev. B.* **2001**, *63*, 155201.
(51) Hofmann, D. M.; Oettinger, K.; Efros, A. L.; Meyer, B. K. *Phys. Rev. B.* **1997**, *55*, 9924−9928.

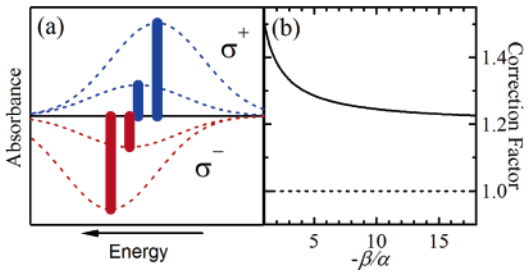

Figure 8. (a) Relative theoretical MCD transition energies and intensities for the Co^{2+}:ZnSe excitonic transition assuming the reported bulk $-\beta/\alpha$ ratio.[26] (b) Correction factor included in eq 4 to account for the four allowed excitonic transitions shown in (a), plotted as a function of $-\beta/\alpha$.

ii. Analysis of MCD Spectra. ΔE_{Zeeman} can be determined from analysis of low-temperature absorption and MCD data. Previously, ΔE_{Zeeman} for other doped and undoped semiconductors has been estimated from such data using eq 3,[15,51] which assumes that the MCD signals arise from the superposition of two equivalent Gaussian bands of opposite sign.

$$\Delta E_{Zeeman} = \frac{2\sigma\Delta A}{A} \tag{3}$$

In eq 3, σ refers to the bandwidth of the Gaussians, ΔA is the maximum excitonic MCD intensity ($\Delta A = A_L - A_R$), and A is the absorbance at the energy of the MCD peak intensity. As described by Figure 7, however, there are four allowed transitions within the derivative-shaped excitonic MCD band. Although the center two transitions are weak and may largely cancel one another in the MCD spectrum (Figure 8a), they both contribute to the absorbance, and their neglect in eq 3 therefore leads to a systematic underestimation of ΔE_{Zeeman}. To account for all four transitions, a correction factor of $CF = (\beta/\alpha + 3)/3(\beta/\alpha - 1)$ must be added to eq 3, yielding eq 4. Numerical simulations have verified the accuracy of eq 4. As shown in Figure 8b, the magnitude of the correction factor depends on the ratio of β/α since the energies of the two central transitions are determined by this ratio. At the typical ratio of $\beta/\alpha = -10$, CF = 21%.

$$\Delta E_{Zeeman} = \frac{2\sigma(\beta/\alpha + 3)}{3(\beta/\alpha - 1)}\frac{\Delta A}{A} \tag{4}$$

For Co^{2+}:ZnSe QDs, determination of ΔE_{Zeeman} is complicated by the presence of a sub-band gap charge-transfer transition. To account for this charge transfer intensity, 6 T MCD spectra were fit using a set of four Gaussians representing the four excitonic Zeeman components with the β/α ratio fixed at its bulk value[26] (Figures 7b and 8a) and with one additional Gaussian representing the charge-transfer transition. Gaussian fitting of the 5 K electronic absorption spectrum provided A and σ for the excitonic transitions, which were then fixed for the MCD fitting. The relative intensities of the four excitonic Gaussians were also fixed at the theoretical ratio of 3:1:−1:−3, a ratio previously confirmed by experiment.[1,50] The charge-transfer Gaussian parameters were also allowed to float in the fitting process but were well constrained by the observable leading edge of this transition in the MCD spectra. The only adjustable parameter for the excitonic MCD intensity was thus ΔE_{Zeeman}, which was varied to reproduce the experimental value of $\Delta A/A$ (eq 4) at the leading (positive) excitonic MCD feature. This approach yielded unique solutions for E_{Zeeman} in each case. ΔE_{Zeeman} determined in this way for three Co^{2+}:ZnSe QDs of different diameters, including those from Figure 5, are presented in Table 1. The error bars represent limits to reasonable fits of the data.[52]

iii. Comparison to Bulk. Table 1 shows that ΔE_{Zeeman} of the Co^{2+}:ZnSe QDs are much lower than those anticipated from bulk sp−d exchange parameters. For example, on the basis of the average of two $N_0(\alpha-\beta)$ values reported for bulk Co^{2+}:ZnSe,[25,26] eq 1 predicts a Zeeman splitting energy of 20.7 meV for the 5.6 nm diameter 0.77% Co^{2+}:ZnSe QDs presented in Figure 5 after accounting for antiferromagnetic Co^{2+} dimer pairing through Poisson statistics,[4] but the experimental value (13.3 meV) is only 64% of this expected value. This discrepancy is well beyond the experimental uncertainty (Table 1). We conclude that instead of an enhancement of ΔE_{Zeeman} by an order of magnitude in the Co^{2+}:ZnSe QDs relative to bulk, as reported for Mn^{2+}:ZnSe QDs,[14] ΔE_{Zeeman} is reduced by ∼40% in the DMS-QDs.

Quantum confinement has been predicted to weaken p−d exchange coupling in DMS-QDs, such as Mn^{2+}:CdTe QDs.[22] The 40% reduction found for Co^{2+}:ZnSe QDs (Table 1) could only be achieved by this mechanism in the strong quantum confinement regime, where $d_{nc} < 2a_B$.[22] With $d_{nc} \approx 2a_B$, the samples in Table 1 are in the weak confinement regime. The effect of quantum confinement on sp−d exchange coupling is predicted to be small in this regime[22] and therefore cannot account for the substantial reduction in ΔE_{Zeeman} in these Co^{2+}:ZnSe QDs relative to bulk.

iv. Dopant Distributions and sp−d Exchange. We propose that the large reduction in ΔE_{Zeeman} observed in the Co^{2+}:ZnSe DMS-QDs relative to bulk Co^{2+}:ZnSe is attributable to the inhomogeneous dopant distribution within the nanocrystals described in Section IV.B. and Figures 4a and 6. The presence of a 2.5 nm diameter undoped core strongly influences the overlap between exciton and dopant wavefunctions, which directly governs the sp−d exchange interactions. To illustrate, the dominant contribution to ΔE_{Zeeman} is $N_0\beta$, which from perturbation theory depends upon the square of the resonance integral between the excitonic hole and the TM^{2+} dopants as described by eq 5.[53] E^- represents the energy associated with transfer of a valence band hole to the TM^{2+} ion (and E^+ for transfer of a valence band electron to TM^{2+}).

$$N_0\beta = -\frac{16\langle\psi_{VB}|\hat{H}_{pd}|\psi_{t_2}\rangle^2}{S}\left[\frac{1}{E^-} + \frac{1}{E^+}\right] \tag{5}$$

This resonance integral is in turn approximately proportional to the spatial overlap of the hole wavefunction with the dopants.[54] The effect of the undoped core on exciton−dopant overlap is illustrated in Figure 9 for a 5.6 nm diameter Co^{2+}:ZnSe QD. The absence of Co^{2+} in the QD cores where the exciton probability is greatest thus disproportionately reduces dopant−exciton overlap. Figure 9a plots the probability distribution of the exciton calculated by estimating its wave function

(52) Additional fits involving inclusion of a positive band to account for the collective MCD contributions of higher-energy states and thereby better reproduce the second (negative) excitonic MCD feature yielded Zeeman splittings within the error bars provided in Table 1, demonstrating that the analysis is relatively insensitive to the details of the fitting procedure.
(53) Bhattacharjee, A. K. *Phys. Rev. B* **1992**, *46*, 5266−5273.
(54) Mulliken, R. S. *J. Chem. Phys.* **1955**, *23*, 1841−1846.

Table 1. Experimental Excitonic Zeeman Splitting Energies and Effective Landé *g* Factors Determined for Various Co^{2+}:ZnSe QD Samples[a]

QD diam (nm)	Co^{2+} (%)	ΔE_{Zeeman} (5 K, 6 T) (meV)	g_{eff} (5 K)[b]	ΔE_{Zeeman} (saturation)[c] exptl (meV)	ΔE_{Zeeman} (saturation)[c] pred[d] (meV)	exptl vs pred (%)	undoped core diam (nm)
5.6	0.77 ± 0.15	13.3 ± 0.8	65 ± 4	15.2 ± 0.9	23.7 ± 4.9	64 ± 14	2.4
4.6	1.30 ± 0.26	19.2 ± 0.8	94 ± 4	22.0 ± 0.9	37.5 ± 8.0	58 ± 13	2.1
4.1	0.61 ± 0.12	10.7 ± 0.5	52 ± 2	12.2 ± 0.6	19.1 ± 4.0	64 ± 14	1.8

[a] Comparison to bulk Zeeman values at the same Co^{2+} concentrations yields predictions of the undoped core diameters in the Co^{2+}:ZnSe QDs. [b] Calculated from 5 K, 1 T Zeeman splitting and $g_{eff} = \Delta E_{Zeeman}/\mu_B H$. [c] A field- and temperature-independent value. [d] From eq 1 using the average of the $N_0(\alpha - \beta)$ values (2.420 and 2.084 eV) reported for bulk Co^{2+}:ZnSe[25,26] and accounting for antiferromagnetic nearest-neighbor interactions.[4]

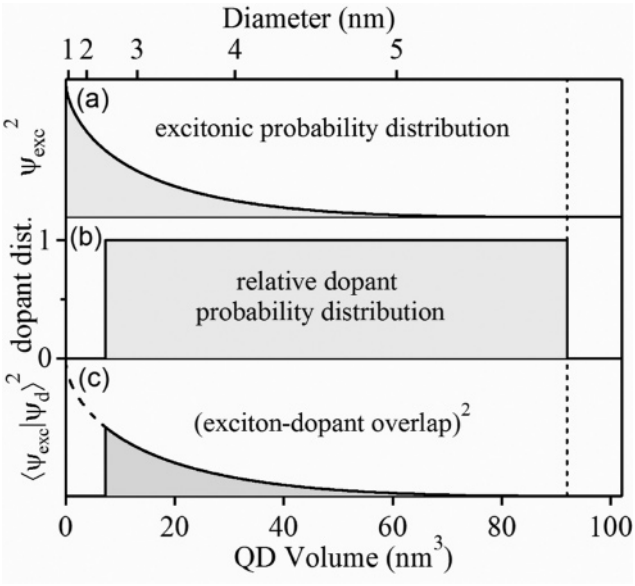

Figure 9. (a) Excitonic probability distribution for 5.6 nm diameter Co^{2+}:ZnSe QDs. (b) The experimental Co^{2+}:ZnSe dopant probability distribution from Figures 4a and 6. (c) The square of the resulting exciton−dopant overlap integral.

in an infinite spherical well,[55] as described previously for conduction band electrons and excitons in QDs.[56] For a 5.6 nm diameter Co^{2+}:ZnSe QD, an undoped core of 2.4 nm diameter would be required to reduce ΔE_{Zeeman} to only 64% of its bulk value. Estimates for the two other Co^{2+}:ZnSe samples in Table 1 yield similar undoped core diameters (Table 1). Importantly, the undoped core diameters estimated from the reduction in ΔE_{Zeeman} are in excellent agreement with those determined independently from analysis of Co^{2+} incorporation during nanocrystal growth (2.5 nm, Figure 4a). This agreement strongly supports the conclusion that the most significant factor reducing ΔE_{Zeeman} in the DMS-QDs relative to bulk is the presence of the undoped QD cores.

v. Zeeman Splittings in DMS-QDs. We propose that direct chemical syntheses of DMS-QDs using monomeric precursors will invariably yield nanocrystals that exhibit lower Zeeman splitting energies than those of the corresponding bulk materials because of dopant exclusion from the critical nuclei.[7,27] For example, ΔE_{Zeeman} reported for Mn^{2+}:CdS QDs grown from solution (3.2 meV)[15] were also smaller than expected (8 meV) from application of eq 2 and bulk $N_0(\alpha - \beta)$ values,[3] although other practical factors may have complicated the analysis of those data. $N_0\beta$ reported for 5 nm diameter Co^{2+}:ZnO nanocrystals (−2.3 eV)[7] is intermediate between two values reported for bulk Co^{2+}:ZnO (−0.8[20] and −3.6 eV[21]), but Co^{2+}:ZnO nanocrystals have only a small undoped core (1 nm diameter), and the large discrepancy between bulk $N_0\beta$ values makes quantitative comparison difficult.

Curiously, ΔE_{Zeeman} reported for 5.3 nm diameter Mn^{2+}:ZnSe QDs (28 meV)[14] was an order of magnitude larger than expected (2.2 meV) from the bulk $N_0(\alpha - \beta)$ value[3] and the reported doping level of only one Mn^{2+} per QD ($x = 0.058\%$, assuming a random position of Mn in the nanocrystal) and was even larger than the maximum possible splitting (22 meV) calculated for the ideal scenario of one Mn^{2+} at the precise QD center.[23] It was proposed in ref 23 on theoretical grounds that the most likely explanation of the discrepancy between reported and calculated ΔE_{Zeeman} values is a greater actual Mn^{2+} content in the experimental Mn^{2+}:ZnSe QDs.[57] Subsequent experimental reports[10,32] from the same researchers do indeed describe significantly higher Mn^{2+} concentrations in Mn^{2+}:ZnSe QDs prepared by the same synthetic procedures (e.g., ∼5−12 Mn^{2+} ions in similarly sized QDs[10,32]). Furthermore, undoped cores were also observed in the Mn^{2+}:ZnSe QDs (see Figure 4a),[10,32] supporting the assertion that dopant exclusion from critical nuclei in chemically prepared DMS-QDs is a general phenomenon.

V. Summary

Colloidal Co^{2+}:ZnSe QDs were synthesized by direct solution chemical methods. Ligand-field electronic absorption spectroscopy confirmed substitutional doping of Co^{2+} into the ZnSe QDs during growth. Absorption spectra collected at different times throughout the syntheses showed that Co^{2+} is absent from the central cores of the QDs. We propose that the undoped cores arise from exclusion of Co^{2+} from the ZnSe critical nuclei, as described previously for Co^{2+}:ZnO.[7,27] Analysis of low-temperature absorption and MCD spectra of three different Co^{2+}:ZnSe QD samples showed E_{Zeeman} consistently ∼40% smaller than expected from bulk Co^{2+}:ZnSe. These reduced ΔE_{Zeeman} values are attributed to the absence of Co^{2+} from the central cores of the QDs, where exciton−dopant overlap would be greatest. Since dopant exclusion from nucleation appears to be a general phenomenon for DMS-QDs grown from monomeric precursors, we propose that ΔE_{Zeeman} will always be smaller in colloidal DMS-QDs grown by these methods than in the corresponding bulk materials. Dopant exclusion from nucleation will thus likely prohibit realization of the enhanced sp−d exchange interactions that can be anticipated in the ideal scenario

(55) Griffiths, D. J. *Introduction to Quantum Mechanics*; Prentice Hall: Upper Saddle River, NJ, 1995.
(56) Brus, L. E. *J. Chem. Phys.* **1984**, *80*, 4403−4409. Fonoberov, V. A.; Balandin, A. A. *Phys. Rev. B* **2004**, *70*.
(57) Note that the equation reported in ref 14 for determination of ΔE_{Zeeman} appears to be a factor of 2 larger than that used previously (eq 3).

of a single dopant at the precise centers of the QDs,[23] and more elaborate synthetic schemes will be required to achieve this motif. More generally, these results demonstrate that chemical issues are more significant than quantum confinement effects in reducing E_{Zeeman} of DMS-QDs prepared by direct chemical routes from monomeric precursors.

Acknowledgment. This research was supported by the National Science Foundation (PECASE DMR-0239325), the Research Corporation, and the Dreyfus Foundation. The authors thank Prof. Pavle V. Radovanovic (U. of Waterloo) for TEM measurements.

JA063425F